NEURODEVELOPMENT

Decoding of position in the developing neural tube from antiparallel morphogen gradients

Marcin Zagorski,[1] Yoji Tabata,[2] Nathalie Brandenberg,[2] Matthias P. Lutolf,[2] Gašper Tkačik,[1] Tobias Bollenbach,[1,3]* James Briscoe,[4]* Anna Kicheva[1,4]*

Like many developing tissues, the vertebrate neural tube is patterned by antiparallel morphogen gradients. To understand how these inputs are interpreted, we measured morphogen signaling and target gene expression in mouse embryos and chick ex vivo assays. From these data, we derived and validated a characteristic decoding map that relates morphogen input to the positional identity of neural progenitors. Analysis of the observed responses indicates that the underlying interpretation strategy minimizes patterning errors in response to the joint input of noisy opposing gradients. We reverse-engineered a transcriptional network that provides a mechanistic basis for the observed cell fate decisions and accounts for the precision and dynamics of pattern formation. Together, our data link opposing gradient dynamics in a growing tissue to precise pattern formation.

In the developing vertebrate neural tube, Sonic hedgehog (Shh) and bone morphogenetic proteins (BMPs) form antiparallel signaling gradients along the dorsoventral (DV) axis (*1*, *2*) (Fig. 1A). Neural progenitors along the entire axis can respond to both Shh and BMP signaling (*3*, *4*). Antiparallel gradients can theoretically provide more precise positional information than single gradients (*5*–*7*), raising the possibility that the precise DV pattern of neural progenitor identities depends on the integration of Shh and BMP signals.

To test this idea, we first measured the BMP and Shh signaling profiles in the growing mouse neural tube (Fig. 1, A to D, figs. S1 and S2, and table S1), using phosphorylated Smad1/5/8 (pSmad) as BMP signaling readout and a transcriptional reporter for Shh signaling (GBS-GFP) (*8*, *9*). The levels of Shh and BMP signaling as a function of the absolute distance to the source did not change appreciably during the first 30 hours of development (Fig. 1, B and C). At later times, the gradient amplitudes decreased (Fig. 1, B and C). Hence, the two signaling gradients had their greatest range at the earliest developmental stages. Subsequently, as the tissue increased in size (*9*), the relative ranges of the gradients decreased (Fig. 1D and fig. S2B).

For the signaling gradients to accurately specify positional identities along the entire DV axis, they must contain sufficiently precise positional information. To examine whether this was the case, we quantified their positional error (*10*, *11*). For each gradient, the positional error was ~1 cell diameter close to the respective morphogen source but increased away from the source (Fig. 1E). Neither the Shh nor the BMP signaling gradient alone provided precise positional information throughout the DV axis. By contrast, the joint positional error (*7*, *10*) resulting from the combined interpretation of both signals was <3 cell diameters at 5 hours and approximately uniform across the DV axis prior to 30 hours of development (Fig. 1E and fig. S2C). After 30 hours, the Shh and BMP signaling levels markedly decreased in the middle of the DV axis and the positional error increased to >20 cell diameters

[1]Institute of Science and Technology IST Austria, 3400 Klosterneuburg, Austria. [2]Institute of Bioengineering, School of Life Sciences, and School of Engineering, Ecole Polytechnique Fédérale de Lausanne, Lausanne, Switzerland. [3]Institute for Theoretical Physics, University of Cologne, Cologne, Germany. [4]Francis Crick Institute, London NW1 1AT, UK.
*Corresponding author. Email: anna.kicheva@ist.ac.at (A.K.); james.briscoe@crick.ac.uk (J.B.); t.bollenbach@uni-koeln.de (T.B.)

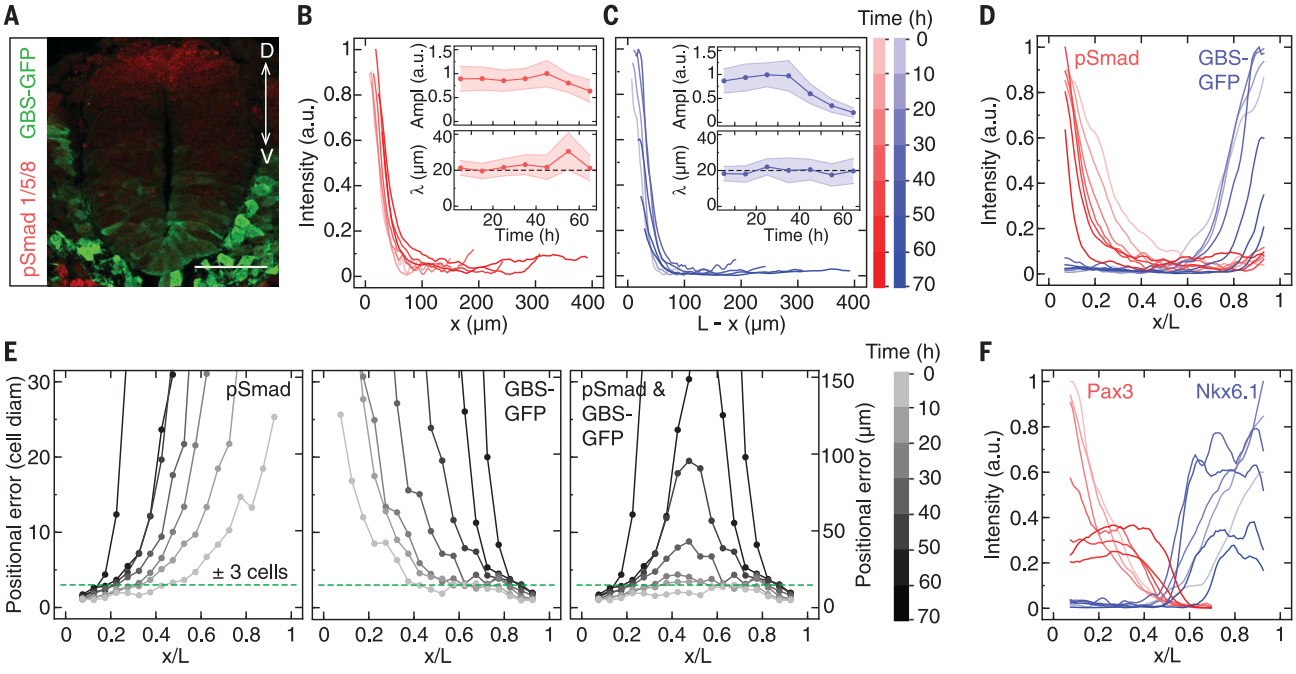

Fig. 1. Dynamics and precision of neural tube patterning. (**A**) Brachial cross section of mouse neural tube at 30 hours, immunostained for GBS-GFP and pSmad1/5/8. Scale bar, 50 μm. D, dorsal; V, ventral. (**B** and **C**) Mean pSmad (B) and GBS-GFP (C) profiles at different developmental stages (sample sizes, table S1). L, total D-V length; x, distance from dorsal pole. (**D**) Mean pSmad and GBS-GFP profiles as a function of relative DV position. Color code is the same as (C). (**E**) Positional error of pSmad and GBS-GFP gradients. The rightmost panel shows the joint positional error of pSmad and GBS-GFP. (**F**) Mean Pax3 and Nkx6.1 expression profiles. Color code is the same as (C).

(Fig. 1E). Thus, together the Shh and BMP gradients can provide precise positional information along the entire DV axis during the first ~30 hours of development.

To assess the precision of pattern, we measured the expression profiles of Nkx6.1 and Pax3. These transcription factors are expressed in distinct progenitor domains (Fig. 1F and fig. S2A) and are part of the morphogen-driven gene regulatory network that controls neuronal subtype specification (*2*). Prior to 30 hours, Nkx6.1 and Pax3 had graded profiles that correlated with Shh and BMP signaling profiles, respectively (Pearson correlation coefficients = 0.9; fig. S2, D to F). After 30 hours, Nkx6.1 and Pax3 expression became steplike and the correlation was lost (fig. S2F). The standard deviations of the Nkx6.1 and Pax3 boundary positions (fig. S2, G and H) after 50 hours were ≤3 cell diameters, whereas the positional error of the signaling gradients was >10 cell diameters (Fig. 1E). This suggests that the gene

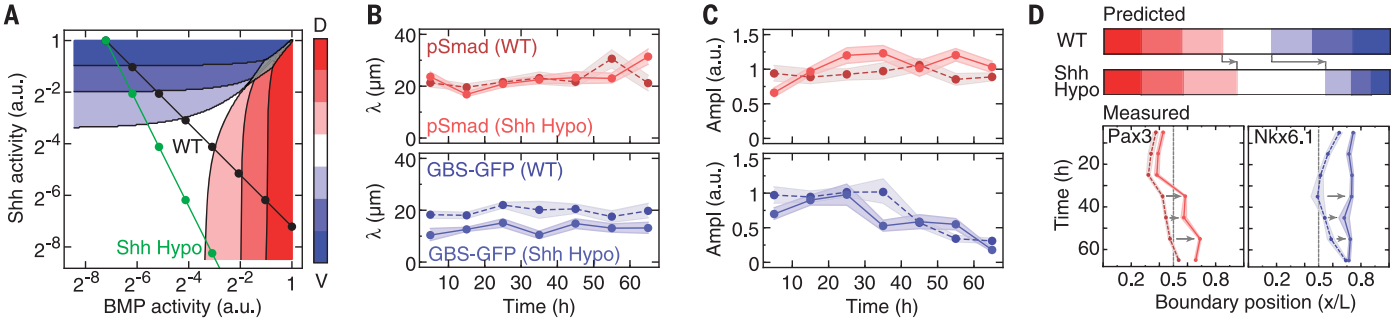

Fig. 2. ML decoding map and predicted pattern in wild-type and Shh^{Hypo} neural tube. (**A**) ML decoding map obtained from wild-type mouse sections at 5 hours, using a parameter-free procedure [(*10*), equation 1]. Colors correspond to predicted positional identities. Mean pSmad and GBS-GFP levels are from exponential fits to the profiles. Black line, wild type; green line, Shh^{Hypo}; black dots, seven equidistant positions along the DV axis. In Shh^{Hypo}, the GBS-GFP profile decay length is half that of the wild type. The probability distributions of DV identities are bimodal in the gray region. (**B**) Exponential decay lengths of pSmad and GBS-GFP for Shh^{Hypo} (solid) and wild-type (dashed) data sets. Shaded regions denote the 95% confidence interval from bootstrapping. (**C**) Amplitudes of pSmad and GBS-GFP profiles, denoted as in (B). (**D**) Top: DV identities predicted from the decoding map in (A). Bottom: Measured Pax3 and Nkx6.1 boundary positions in Shh^{Hypo} (solid line) are shifted ventrally relative to the wild type (dashed line).

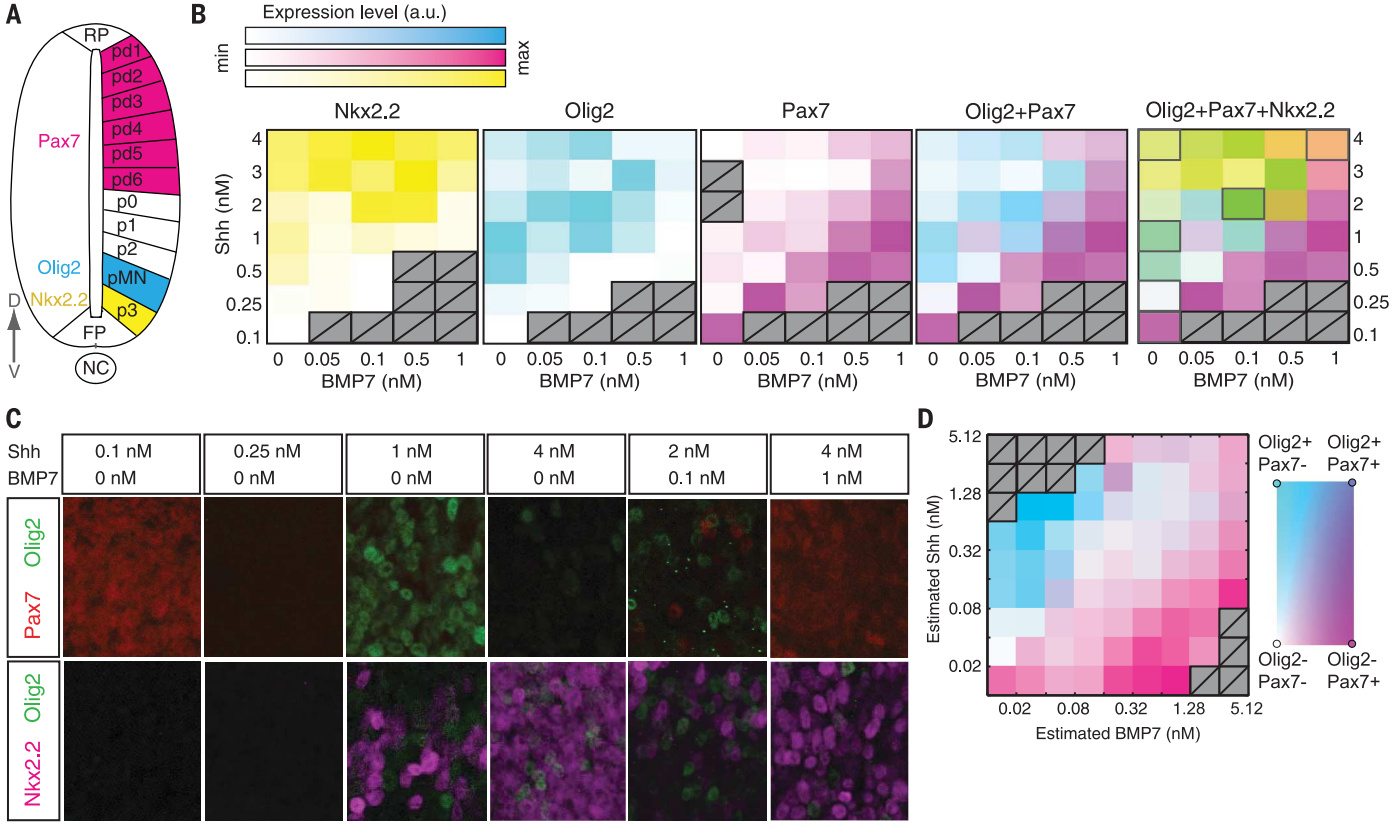

Fig. 3. Response of chick neural plate explants to Shh and BMP7. (**A**) DV expression domains of indicated genes [see also (*2*)]. (**B**) Mean proportion of explant area positive for Pax7 (magenta), Olig2 (cyan), or Nkx2.2 (yellow) after culture in the indicated Shh and BMP7 concentrations for 24 hours (sample sizes, table S2). The rightmost two panels are overlays. (**C**) Representative images for the conditions outlined in gray in the last panel of (B). (**D**) Proportion of Pax7$^+$ and Olig2$^+$ pixels as a function of the calibrated Shh and BMP7 concentrations for a set of explants cultured in microfluidic devices. Sample size, mean per bin n = 4.7 (range, 2 to 14). Hatched regions were not sampled.

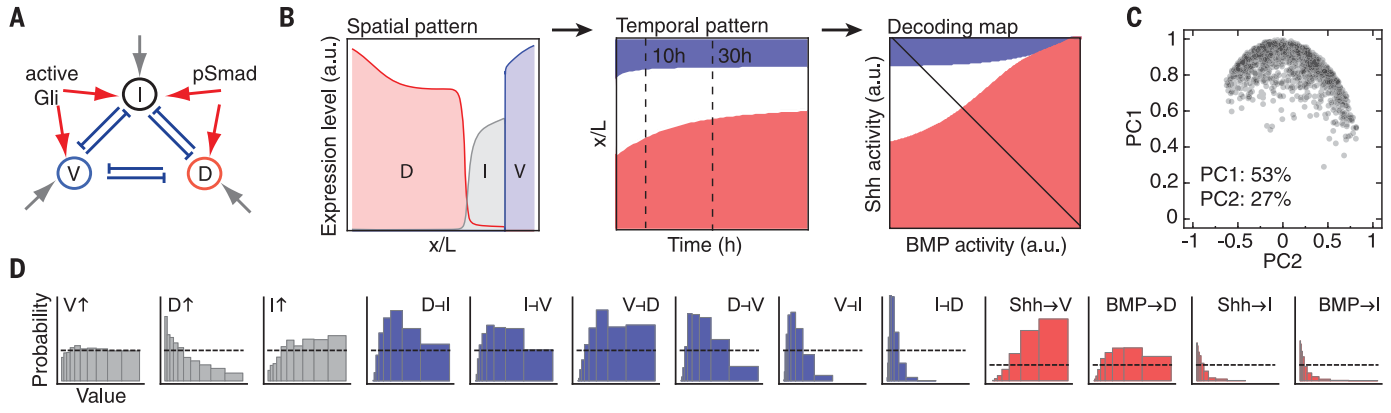

Fig. 4. Computational screen for morphogen-controlled transcriptional networks. (**A**) Morphogen-driven transcriptional network in the neural tube. Shh and BMP signaling activate ventral (V), intermediate (I), and dorsal (D) target transcription factors. Gray arrows denote uniform activating inputs. Degradation is not depicted. (**B**) Criteria of the computational screen. (**C**) Principal components analysis of successful parameter sets. Contributions of the first two principal components to the total variation are indicated. (**D**) Distribution of parameter values for solutions that pass the screen. Uniform random distributions (dashed lines) are shown for comparison.

expression domains are established at early developmental times and then become independent of morphogen signaling after 30 hours (*9*).

The similarity in the precision of signaling profiles at early times (Fig. 1E) and target gene boundary positions (fig. S2H) suggested that cells interpret the signals in a way that minimizes pattern imprecision. Theoretical studies (*7*, *12*) have shown that maximum likelihood (ML) estimation of position from the joint morphogen signaling levels is a decoding strategy that ensures minimum positional imprecision, given noisy gradients (*10*). ML estimation uses the observed mean and variance of a set of signaling profiles to determine the probability distributions of positional identities that correspond to any given combination of Shh and BMP signaling [(*10*), equation 1]. The maxima of these probability distributions represent a ML decoding map. Thus, if the interpretation mechanism in the neural tube represents an optimal decoding strategy that minimizes imprecision, then the positional identities adopted for arbitrary combinations of Shh and BMP signaling would be the same as predicted by ML estimation. To test this, we used the observed signaling profiles at 5 hours to calculate the distributions of positional identities for any combination of Shh and BMP signaling (fig. S3) (*10*) and determined the ML decoding map (Fig. 2A).

Inspection of the map suggested that the pattern would shift for signaling profiles different from those of the wild type. Shh-GFP homozygous embryos (Shh^{Hypo}) are hypomorphic for Shh signaling (*13*) (fig. S4). In these embryos, the amplitudes of the signaling profiles and the absolute pSmad decay length were similar to those of the wild type for most time points (Fig. 2, B and C, and fig. S5). However, the decay length of the Shh signaling gradient was smaller than in the wild type, both in absolute units and relative to tissue size (*t*-test P value < 0.005; Fig. 2B and fig. S5B). Hence, at 5 hours of development, the combined levels of Shh and BMP signaling along the DV axis in the Shh^{Hypo} differed from those observed in the wild type (Fig. 2A). In the ML decoding map, equivalent positions along the DV axis of Shh^{Hypo} and the wild type are associated with different positional identities (Fig. 2, A and D). These predicted shifts are consistent with the experimentally observed ventral shifts of the Nkx6.1 and Pax3 boundaries in Shh^{Hypo} relative to the wild type (Fig. 2D).

A notable feature of the ML decoding map is that intermediate identities are obtained only for low levels of both morphogens (Fig. 2A and fig. S3A). At high levels of both signals, unlike the unimodal distributions of positional identities obtained at most Shh/BMP combinations, the distributions are bimodal, with a low probability of adopting intermediate identities (fig. S3B). To test this feature of the map, we measured the response of explants isolated from the intermediate region of the chick neural plate to defined concentrations of Shh and BMP7 after 24 hours of culture (Fig. 3, A to C, and fig. S6) (*10*). We assayed the expression of target genes that subdivide the DV axis into distinct domains (Fig. 3A and fig. S6A). Consistent with previous results (*14*), in the absence of BMP, addition of 1 nM Shh resulted in explants expressing predominantly Olig2, whereas Nkx2.2 was expressed in most cells exposed to 4 nM Shh (Fig. 3, B and C). In response to low or no Shh, explants acquired dorsal $Pax7^+$ fates (*3*). Low levels of both Shh and BMP (0.5 nM Shh, 0.05 nM BMP) resulted in explants adopting an intermediate identity, marked by the expression of factors such as Dbx1 and Nkx6.1 (fig. S6), but not Pax7, Olig2, or Nkx2.2 (Fig. 3, B and C).

Exposure to high concentrations of both Shh and BMP resulted in a different outcome. Explants treated with 2 to 4 nM Shh and 0.5 to 1 nM BMP contained a mixture of cells with dorsal ($Pax7^+$) and ventral identities ($Nkx2.2^+$ or $Olig2^+$) (Fig. 3, B and C) but no $Dbx1^+$ intermediate identities (fig. S6 and table S2). Dorsal and ventral markers were not coexpressed in the same cell but were observed in adjacent cells (Fig. 3C), indicating that individual cells make a definitive decision between ventral or dorsal identities. We validated these responses using a novel microfluidic device that allows us to culture explants in defined antiparallel gradients (*10*) (figs. S7 and S8). A region of intermediate identities was apparent at low Shh/BMP concentrations (~0.05 nM Shh, ~0.02 nM BMP7), whereas intermixed or directly adjacent $Pax7^+$ and $Olig2^+$ cells occurred at high concentrations (Fig. 3D). Thus, the ML decoding map captures the experimentally observed distinct responses to low and high signaling levels of both morphogens and provides a characteristic signature of a strategy that minimizes the imprecision of pattern. This rules out mechanisms such as interpretation of the difference or the ratio of the two signals [e.g., (*15*)], which would generate similar responses at low and high levels of signaling (fig. S9).

The decoding map is a phenomenological model of patterning that does not describe a specific molecular mechanism. Thus, the question remains as to how the observed decoding strategy is molecularly implemented. We hypothesized that the observed responses can be explained by the dynamics of the morphogen-controlled transcriptional network in the neural tube. To test this, we extracted a core network for the central region of the neural tube (Fig. 4A). This region expresses Dbx1/2, which is adjacent to the Nkx6.1/6.2 domain ventrally and the Pax3/7 domain dorsally (*16*–*18*). Cross-repressive interactions between pairs of these factors have been identified (*16*–*20*). We therefore conceived a network composed of dorsal (D; e.g., Pax3), intermediate (I; e.g., Dbx2), and ventral (V; e.g., Nkx6.1) transcription factors and used this as the basis of a computational screen (*21*) for networks that would reproduce the experimental observations (Fig. 4B) (*10*). Using the measured signaling profiles as input (Fig. 1D), we obtained 1221 parameter sets, out of 600 million randomly generated, that recapitulated the key experimental observations and reproduced the characteristic decoding map. Principal components analysis did not reveal distinct clusters (Fig. 4C); for 99.6% of the sets, interpolating

parameter values between at least two sets resulted in solutions that passed the screening criteria. This suggested a connected parameter subspace. Many of the successful solutions had three stable fixed points (34%), were insensitive to initial conditions, and matched the measured precision of target gene boundaries (fig. S10).

The successful solutions displayed common features. The activation of I by morphogen signaling was weaker than the activation of V by Shh and D by BMP (Fig. 4D) and was not required (table S3). The width of the I stripe correlated negatively with the strength of I repression by D and V, and also correlated negatively with the strength of D and V activation by morphogens (fig. S10C). Thus, high levels of signaling induce V and D fates, which in turn repress the I fate. For the intermediate identities to be specified and maintained, the levels of signaling of both morphogens have to be low. In this way, the transcriptional network produces the signature of the ML decoding map. All repressive cross-interactions were required (table S3) and tightly constrained (Fig. 4D and fig. S10D). Cross-repressive interactions generate multistability of gene expression, and this could explain how pattern is maintained independent of morphogen signaling at later times. Simulating the network dynamics with signaling input restricted to progressively shorter periods revealed that signaling is essential only during the first 15 hours (fig. S10E).

Finally, the network model also predicted the effect of genetic perturbations that were not part of the screening criteria. Shh null mutants lack ventral and most intermediate identities (*22*, *23*), whereas embryos lacking Shh and Gli3, the main Gli repressor, recover some ventral cell types and express Nkx6.1 (*23*, *24*). Simulations of the VID network were consistent with these observations (fig. S11).

Transcriptional networks are versatile (*25*) and can support robust information processing (*26*). In the mouse neural tube, we uncovered a transcriptional network that allows neural progenitors to integrate information from the opposing gradients. The resulting response has the characteristics of a decoding strategy that maximizes the precision of pattern (fig. S12). Thus, the regulatory network integrates two graded inputs to precisely measure location in a developing tissue and maintains accurate pattern as the tissue grows.

REFERENCES AND NOTES

1. J. Briscoe, S. Small, *Development* **142**, 3996–4009 (2015).
2. W. A. Alaynick, T. M. Jessell, S. L. Pfaff, *Cell* **146**, 178–178.e1 (2011).
3. K. F. Liem Jr., T. M. Jessell, J. Briscoe, *Development* **127**, 4855–4866 (2000).
4. C. M. Mizutani, N. Meyer, H. Roelink, E. Bier, *PLOS Biol.* **4**, e313 (2006).
5. Y. Morishita, Y. Iwasa, *Phys. Rev. E* **79**, 061905 (2009).
6. J. O. Dubuis, G. Tkačik, E. F. Wieschaus, T. Gregor, W. Bialek, *Proc. Natl. Acad. Sci. U.S.A.* **110**, 16301–16308 (2013).
7. G. Tkačik, J. O. Dubuis, M. D. Petkova, T. Gregor, *Genetics* **199**, 39–59 (2015).
8. N. Balaskas *et al.*, *Cell* **148**, 273–284 (2012).
9. A. Kicheva *et al.*, *Science* **345**, 1254927 (2014).
10. See supplementary materials.
11. T. Bollenbach *et al.*, *Development* **135**, 1137–1146 (2008).
12. Y. Morishita, Y. Iwasa, *Biophys. J.* **101**, 2324–2335 (2011).
13. C. E. Chamberlain, J. Jeong, C. Guo, B. L. Allen, A. P. McMahon, *Development* **135**, 1097–1106 (2008).
14. E. Dessaud *et al.*, *Nature* **450**, 717–720 (2007).
15. P. McHale, W.-J. Rappel, H. Levine, *Phys. Biol.* **3**, 107–120 (2006).
16. J. Briscoe, A. Pierani, T. M. Jessell, J. Ericson, *Cell* **101**, 435–445 (2000).
17. S. Moore *et al.*, *PLOS Genet.* **9**, e1003811 (2013).
18. A. Vallstedt *et al.*, *Neuron* **31**, 743–755 (2001).
19. M. Sander *et al.*, *Genes Dev.* **14**, 2134–2139 (2000).
20. T. Oosterveen *et al.*, *Dev. Cell* **23**, 1006–1019 (2012).
21. D. Ben-Zvi, B. Z. Shilo, A. Fainsod, N. Barkai, *Nature* **453**, 1205–1211 (2008).
22. C. Chiang *et al.*, *Nature* **383**, 407–413 (1996).
23. Y. Litingtung, C. Chiang, *Nat. Neurosci.* **3**, 979–985 (2000).
24. M. Persson *et al.*, *Genes Dev.* **16**, 2865–2878 (2002).
25. J. Cotterell, J. Sharpe, *Mol. Syst. Biol.* **6**, 425 (2010).
26. G. Tkačik, W. Bialek, *Annu. Rev. Condens. Matter Phys.* **7**, 89–117 (2016).

ACKNOWLEDGMENTS

We thank T. Jessell and E. Laufer for antibodies. Supported by IST Austria (M.Z., G.T., T.B., and A.K.); Austrian Science Fund grant FWF P 28844 (G.T.); the European Research Council under European Union (EU) Horizon 2020 research and innovation program grant 680037 (M.Z. and A.K.); People Programme (Marie Curie) of the EU Seventh Framework Programme grant REA 291734 (M.Z.); the Francis Crick Institute, which receives its core funding from Cancer Research UK grant FC001051, UK Medical Research Council grant FC001051, and Wellcome Trust grants FC001051 and WT098326MA (J.B. and A.K.); and ERC grant StG_311422 and the EU Seventh Framework HEALTH research program PluriMes (www.plurimes.eu) (Y.T., N.B., and M.P.L.). Supplement contains additional data.

SUPPLEMENTARY MATERIALS

www.sciencemag.org/content/356/6345/1379/suppl/DC1
Materials and Methods
Figs. S1 to S12
Tables S1 to S3
References (*27*–*34*)

13 December 2016; accepted 1 June 2017
10.1126/science.aam5887

Decoding of position in the developing neural tube from antiparallel morphogen gradients

Marcin Zagorski, Yoji Tabata, Nathalie Brandenberg, Matthias P. Lutolf, Gasper Tkacik, Tobias Bollenbach, James Briscoe and Anna Kicheva

Science **356** (6345), 1379-1383.
DOI: 10.1126/science.aam5887

Building the neural tube

The development of the neural tube is regulated by a pair of morphogens acting in opposing gradients. The mature neural tube is built from a variety of different cell types organized in a consistent dorsal-ventral pattern. Zagorski *et al.* asked how this pattern is defined in a reproducible way from individual to individual. The morphogens define positions most accurately toward the top of their respective gradients, but things get a bit messy in the middle. Modeling the gene regulatory network's response as a maximum likelihood estimation from the combined input of both morphogens, however, succeeds at defining even the intermediate positions. Thus, the computation of position by the gene regulatory network establishes accurate tissue patterning despite messy inputs.

Science, this issue p. 1379